HOSTED BY

ELSEVIER

CrossMark

Available online at www.sciencedirect.com

ScienceDirect

Progress in Natural Science: Materials International 24 (2014) 378–387

Progress in Natural Science Materials International

www.elsevier.com/locate/pnsmi
www.sciencedirect.com

Original Research

Growth, structural, optical, thermal and dielectric properties of a novel semi-organic nonlinear optical crystal: Dichloro-diglycine zinc II

B. Uma[a], Rajnikant[b], K. Sakthi Murugesan[d], S. Krishnan[c], B. Milton Boaz[d,*]

[a]Department of Physics, R.M.K. Engineering College, Kavaraipettai 601206, India
[b]X-ray Crystallography Laboratory, Post-Graduate Department of Physics & Electronics, University of Jammu, Jammu Tawi 180006, India
[c]Department of Physics, B.S.Abdur Rehman University, Vandalur, Chennai 600048, India
[d]PG and Research Department of Physics, Presidency College, Chennai 600005, India

Received 18 July 2013; accepted 9 May 2014
Available online 15 August 2014

Abstract

Dichloro-diglycine zinc II (DCDGZ II), a semi-organic nonlinear optical material has been synthesized and single crystals were grown from the aqueous solution up to dimensions $20 \times 10 \times 3$ mm^3. The title compound, DCDGZ II ($C_4H_{10}Cl_2N_2O_4Zn \cdot H_2O$) crystallizes into monoclinic structure with the space group of C2/c. The unit-cell parameters were found to be $a=14.4191(7)$, $b=6.9180(2)$, $c=12.9452(6)$ Å and $Z=4$. In the crystal structure, DCDGZ II layer is building up alternatingly with layers of water in which the zinc ions lie on a twofold axis. Theoretical calculations for polarizability, which are useful for device fabrication were made using Clausius–Mosotti equation and Penn analysis and the results were compared. Fourier transform infrared (FTIR) spectroscopic studies were performed for the identification of the different functional groups presented in the compound. The UV–vis–NIR absorption spectrum reveals that the lower UV cut-off wavelength is 240 nm. The optical band gap of the crystal was estimated as 2.2 eV. The surface morphology, thermal behaviour, dielectric properties have been studied using SEM, TG/DTA and LCR HITESTER analyzer. The nonlinear optical property of the crystal was also confirmed using Kurtz powder technique.

Keywords: Crystal structure; Growth from solutions; Characterization; Non-linear optic materials

1. Introduction

Over recent years, high efficient nonlinear optical (NLO) materials has obtained more attention due to their potential applications, such as high-speed information processing, optical communications, optical communications, and optical data storage [1–3]. Among the class of NLO materials, the inorganic material possesses high melting point, high mechanical strength and high degree of chemical inertness. But, their optical nonlinearity is poor. Whereas, organic compounds are having high nonlinearity due to the weak van der Waals and hydrogen bonds and possess high degree of delocalization. However, the difficulty is to grow the large and optically good quality single crystals for device applications.

These drawbacks of organic and inorganic crystals may be overcome by semi-organic materials, which share both the properties of inorganic and organic materials [4]. Several semi-organic crystals belonging to aminoacid, thiourea and nitrophenol are exhibiting NLO properties [5–9]. However, in the family of aminoacids glycine plays a major role in forming better size and efficient semiorganic NLO crystals. Unlike the other aminoacids, glycine has three polymorphic crystalline forms α, β and γ. Also glycine and its methylated analogues form complexes with mineral acids exhibiting interesting physical properties like ferroelastic, ferroelectric or antiferroelectric behaviour [10]. The configuration of glycine ions interconnected by short O–H···O hydrogen bonds are regarded as particularly important for the ferroelectric behaviour of this crystal and the molecules are held

*Corresponding author.
E-mail address: miltonboazcm@yahoo.co.in (B.M. Boaz).
Peer review under responsibility of Chinese Materials Research Society.

http://dx.doi.org/10.1016/j.pnsc.2014.07.001

together by a network of N–H···X, N–H···O and O–H···O hydrogen bonds which are similar to the structures of diglycine hydrochloride [11], hyrdrobromide [12], hydroiodide [13] and disarcosine hydrobromide [14].

Though, dichloro-diglycine zinc II (DCDGZ II) was reported few times as diglycine zinc chloride and dichloride diglycine zinc dihydrate with characterization [15–17], the main difference between the above crystals with DCDGZ II is monohydrate form. Hence, much interest is focused even now due to its widespread application in optical parametric amplifiers, optical switching, optical communications, image processing and photonics [18]. In the present investigation, we report the growth aspects and the characterization studies such as structural, FTIR, UV–vis–NIR absorption, scanning electron microscope, TG/DTA, NLO and dielectric measurements. Theoretical calculations for polarizability were also made using Clausius–Mosotti equation and Penn analysis and their results are compared.

2. Experimental procedure

2.1. Synthesis and crystal growth

The starting materials glycine and zinc chloride (analytical grade reagents) were taken in the molar ratio 2:1. The calculated amounts of salts were dissolved in deionised water at room temperature. In the reaction process one mole of zinc chloride solution was added drop by drop slowly to the already prepared solution. The final solution thus obtained after six hours of continuous stirring was left to evaporate at room temperature. The purity of the synthesized salt was improved further by successive recrystallization process in order to get defect-free seed crystal. The seed obtained from the saturated slow evaporated solution of the synthesized salt was used for the bulk growth. After the period of 35 days, optically transparent crystals having dimensions $20 \times 10 \times 3$ mm^3 have been harvested from the parent solution. The photograph of the grown crystal is shown in Fig. 1.

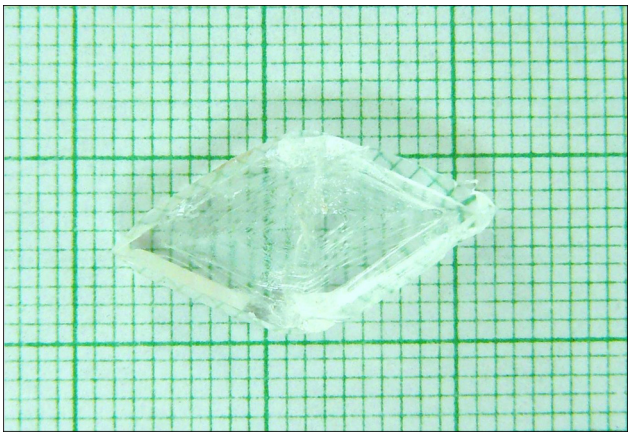

Fig. 1. As grown crystal of dichloro-diglycine zinc II (DCDGZ II).

2.2. Characterization

The single crystal of DCDGZ II was subjected to single crystal X-ray diffraction using ENRAF NONIUS CAD4 X-RAY Diffractometer to determine the structural details. The FTIR spectrum was recorded in the range of 400–4000 cm^{-1} using BRUKKER IFS 66 FTIR spectrometer in order to confirm the presence of functional groups. The optical absorption spectrum was measured in the range of 200–2500 nm using JASCO V-650 UV–vis–NIR spectrophotometer. Surface analysis was carried out through Hitachi–S–3400N scanning electron microscope to determine the smoothness of the surface. Thermal stability of the sample was examined by TG–DTA analysis using TGA Q500 V 20.10 instrument. The dielectric study has been carried out using the instrument of HIOKI 3532-50 LCR HITESTER. The relative second harmonic generation was carried out by Kurtz powder technique in order to confirm nonlinearity of the crystal.

3. Results and discussion

3.1. X-ray crystallographic studies

3.1.1. Single crystal diffraction

The single crystal X-ray diffraction has been carried out using CCD area-detector diffractometer (X'calibur system – [19]) which is equipped with graphite monochromated MoKα radiation (λ=0.71073 Å). The cell dimensions were determined by least-squares fit of angular settings of 7790 reflections in the θ range 4.1227–28.9484° A total number of 9427 reflections were collected of which 1078 reflections were treated as observed ($I > 2\sigma(I)$). Data were corrected for Lorentz, polarization and absorption factors. The structure was solved by direct methods using SHELXS97. Full-matrix least-squares refinement was carried out by using SHELXL97 software [20]. All the hydrogen atoms were located from a difference electron density map and their positional and isotropic thermal parameters were included in the refinement. The final refinement cycle yielded an R-factor of 0.0156 [$wR(F^2)$=0.0414] for the observed data. The residual electron density ranges from −0.318 to 0.294 eÅ^{-3}. Atomic scattering factors were taken from International Tables for X-ray Crystallography (1992, Vol. C, Tables 4.2.6.8 and 6.1.1.4). Table 1 shows the crystal data and other experimental details. Bond lengths (Å), bond angles (deg) and torsion angles for non-hydrogen atoms are presented in Table 2.

An ORTEP view of the title compound with atomic labelling is shown in Fig. 2 [21]. The geometry of the molecule was calculated using PARST [22] and PLATON software [23]. All H atoms bound to nitrogen are engaged in N–H···Cl and N–H···O interactions [lesser than (DHA) greater than 135°] Table 3, which lead to the formation of supramolecular structure Fig. 3. In the glycine group, the bond lengths and angles are N1–C2 [1.469(2) Å], C2–C3 [1.512(2) Å], N1–C2–C3 [113.06(12)°] and N1–C2–C3–O4 [−14.5(2)°]. The packing of molecules in the unit cell can be described as layers of

Table 1
Crystallographic data and other experimental details.

Crystal description	White block
Crystal size	$0.30 \times 0.20 \times 0.20$ mm^3
Empirical formula	$C_4H_{10}Cl_2N_2O_4Zn$, (H_2O)
Formula weight	322.44
Measurement	*X'calibur system–Oxford diffraction*
Radiation, wavelength	MoKα, 0.71073 Å
Cell measurement temperature	293(2) K
Unit cell dimensions	$a=14.4191(7)$, $b=6.9180(2)$ $c=12.9452(6)$ Å, $\beta=117.867(6)^\circ$
Crystal system	Monoclinic
Space group	C2/c
Unit cell volume	1141.55(8) Å^3
Density (calculated)	1.876Mg m^{-3}
No. of molecules per unit cell, Z	4
Absorption coefficient	2.630 mm^{-1}
$F(000)$	656
Refinement of unit cell	7790 reflections for $4.1227^\circ < \theta < 28.9484^\circ$
Scan mode	ω Scans
Range for entire data collection	$4.13^\circ < \theta < 25.99^\circ$
Range of indices	$h=-17$ to 17, $k=-8$ to 8, $l=-15$ to 15
Reflections collected/unique	9427/1115
Reflections observed ($I > 2\sigma(I)$)	1078
R_{int}	0.0361
R_{sigma}	0.0175
Structure determination	Direct methods
Refinement	Full-matrix least-squares on F^2
No. of parameters refined	98
Final R-factor	0.0156
$wR(F^2)$	0.0409
Goodness-of-fit	1.051
$(\Delta/\sigma)_{max}$	0.001 for y Zn1
Final residual electron density	$-0.318 < \Delta\rho < 0.294$ eÅ^{-3}
Software for structure solution	SHELXS97
Software for refinement	SHELXL97
Software for molecular plotting	ORTEP-3, PLATON
Software for geometrical calculations	PLATON, PARST

Table 2
Bond lengths (Å) and bond angles (deg) and torsion angles for non-hydrogen atoms **(e.s.d.'s are given in parentheses)**.

Bond distances			
Zn1–O4	1.9796(10)	Zn1–Cl2	2.2345(4)
O4–C3	1.2667(18)	O5–C3	1.2405(18)
N1–C2	1.469(2)	C2–C3	1.512(2)
Bond angles			
O4–Zn1–O4	97.69(7)	O4–Zn1–Cl2	118.89(3)
Cl2–Zn1–Cl2	106.61(2)	C3–O4–Zn1	120.65(10)
N1–C2–C3	113.06(12)	O5–C3–O4	126.35(14)
O5–C3–C2	117.54(13)	O4–C3–C2	116.11(13)
Torsion angles			
Cl2–Zn1–O4–C3	−56.59(12)	Zn1–O4–C3–O5	20.7(2)
Zn1–O4–C3–C2	−158.49(10)	N1–C2–C3–O5	166.20(14)
N1–C2–C3–O4	−14.5(2)		

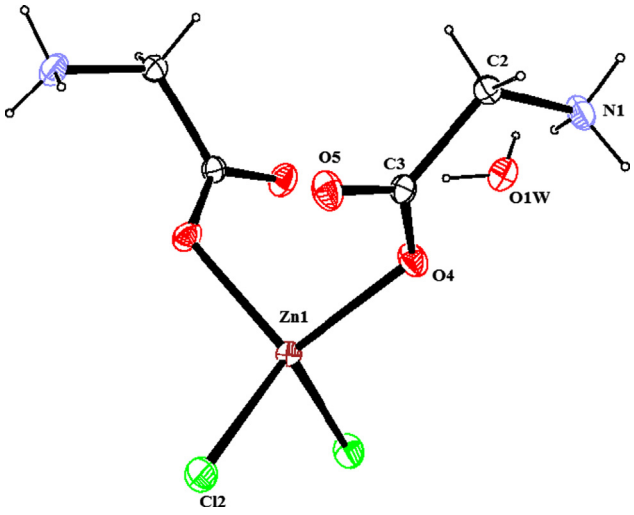

Fig. 2. ORTEP view of the molecule, showing the atom-labelling scheme.

dichloro-diglycine zinc II moiety alternating with layers of water Fig. 4. In the crystal structure, N–H···Cl, N–H···O and O–H···O interactions are present Table 3. The CIF for this structure has been deposited at Cambridge Crystal Data Centre (CCDC no: 882526). From the X-ray diffraction data, it is observed that the DCDGZ II crystals are monoclinic and belong to C2/c space group. The crystal structure was in good

Table 3
Geometry of intra- and intermolecular hydrogen bonds.

DH···A	DH(Å)	H···A (Å)	D···A (Å)	[DH···A (deg)]
N1–H11···O1W	0.88(2)	2.873(2)	2.00(2)	177(2)
N1–H12···O5^{i}	0.87(3)	2.42(2)	3.173(2)	145(2)
N1–H12···Cl2^{ii}	0.87(3)	2.63(3)	3.181(2)	122(2)
O1W–H1W···O5^{iii}	0.83(2)	2.06(2)	2.887(2)	173(3)
N1–H13···O1W^{iv}	0.82(2)	2.08(2)	2.890(2)	169(2)
O1W–H2W···O5^{v}	0.75(3)	2.914(2)	2.166(3)	173(3)

Symmetry code: (i) $-x+1,-y+1,-z$; (ii) $x+1/2,+y-1/2,+z$; (iii) $x+1/2,-y+1/2,+z+1/2$; (iv) $-x+1/2+1,+y-1/2,-z+1/2$; (iv) $-x+1,+y,-z+1/2$.

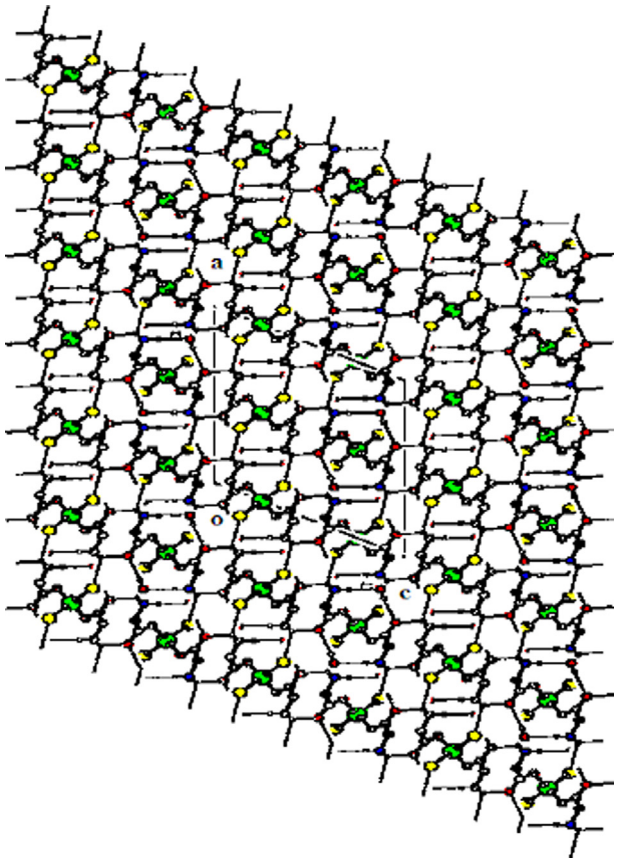

Fig. 3. The packing arrangement of molecules viewed down the *b*-axis.

agreement with the reported structure other than the water molecule [16].

3.1.2. Theoretical measurements

The valence electron plasma energy $\hbar\omega_P$, is given by

$$\hbar\omega_P = 28.8\left(\frac{Z_\rho}{M}\right)^{1/2} \quad (1)$$

where $Z=((4Z_C)+(12Z_H)+(2Z_N)+(5Z_O)+(2Z_{Cl})+(1Z_{Zn}))=84$ is the total number of valence electrons, ρ is the density and M is the molecular weight of the crystal. The Penn gap and the Fermi energy are explicitly dependent on the $\hbar\omega_P$ [24] which

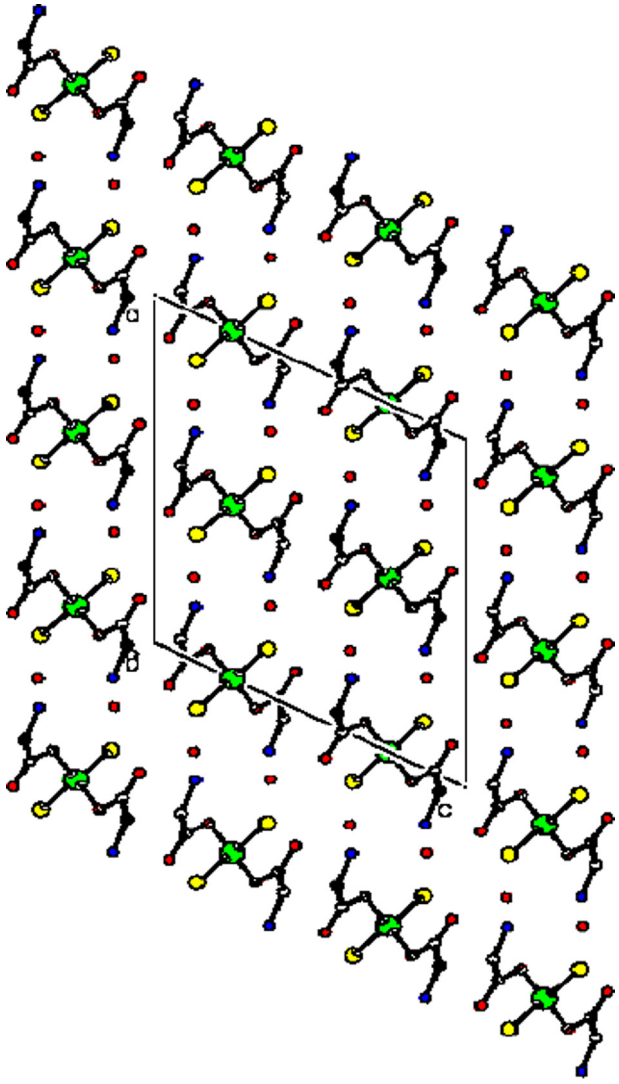

Fig. 4. Packing of molecules in the unit cell as layers of dichloro-diglycine zinc II moiety and water.

are given by

$$E_P = \frac{\hbar\omega_P}{(\varepsilon_\infty - 1)^{1/2}} \quad (2)$$

$$E_F = 0.2948\,(\hbar\omega_P)^{4/3} \quad (3)$$

The molecular polarizability, 'α' is obtained by using the relation [25]

$$\alpha = \left\lfloor \frac{(\hbar\omega_P)^2 s_0}{(\hbar\omega_P)^2 s_0 + 3E_P{}^2} \right\rfloor \frac{M}{\rho} 0.396 \times 10^{-24}\ \mathrm{cm}^{-1} \quad (4)$$

where S_0 is a constant for the material, which is given by

$$S_0 = 1 - \left[\frac{E_P}{4E_F}\right] + \frac{1}{3}\left[\frac{E_P}{4E_F}\right]^2 \quad (5)$$

The value of α so obtained agrees well with that of the Clausius–Mossotti equation, which is given by the relation

$$\alpha = \frac{3M}{4\pi N_a \rho}\left(\frac{\varepsilon_\infty - 1}{\varepsilon_\infty + 2}\right) \quad (6)$$

All these calculated theoretical data for the grown crystal are presented in Table 4.

3.2. Fourier transform infrared (FTIR) spectroscopic analysis

The FTIR analysis of the samples was carried out between 4000 and 400 cm^{-1} using the Bruker IFS 66, FTIR spectrometer and the resultant spectrum is shown in Fig. 5. Glycine exists as zwitterions in which the carboxyl group is present as carboxylate ion and the amino group exists as ammonium ion. Transmission due to the carboxyl group of free glycine was observed at 504.2, 893 and 1605 cm^{-1}. In the DCDGZ II these peaks were shifted to 553.47, 903.969 and 1635.82 cm^{-1}. The peak at 903.969 cm^{-1} corresponds to C–C stretching vibrations. Similarly, the transmission peaks for the NH_3^+ group of free glycine were observed at 1110, 1333 and 3175 cm^{-1}. But in DCDGZ II these peaks were shifted to 1139.72, 1342.7 and 3199.81 cm^{-1}. This observation confirms that glycine exists in zwitterionic form. The involvement of NH_3^+ in hydrogen bonding is evident by the fine structure of the band in the lower region. In the absorption spectra of DCDGZ II the wave number 1139.72 cm^{-1} come from the split of one broad absorption band. The rocking modes of NH_3^+ group in α form crystal of glycine were observed in the same wave number region [26]. In the FTIR spectrum of DCDGZ II, the NH_2 rocking vibration was observed at 1635.82. The peak at 1043.78 cm^{-1} corresponds to CCN stretching vibrations. The peaks at 3455.81 and 3199.81 cm^{-1} correspond to O–H asymmetric stretching vibrations. The COO^- symmetric vibrations were observed in 1521.08 and 706.783 cm^{-1}. The wave numbers 2723.96, 1342.7 and 903.969 cm^{-1} represents CH_2 symmetric stretching, CH_2 wagging, CH_2 rocking vibrations respectively. CH_2 and C–O stretching vibrations were observed at 2643.93 and 1395.73 cm^{-1}. The FTIR spectral data of the DCDGZ II crystal is tabulated in Table 5 is in good agreement with the reported values [15–17].

Table 4
Theoretical measurements of DCDGZ II crystal.

Parameters	Values
Plasma energy	22.62 (eV)
Penn gap energy	10.66 (eV)
Fermi energy	18.85 (eV)
Polarizability	
By Penn analysis	3.85×10^{-23} (cm^3)
By Clausius–Mossotti equation	4.08×10^{-23} (cm^3)

Table 5
FTIR spectral ata of DCDGZ II crystal.

Wave number (cm^{-1})	Assignments
3455.81	O–H asymmetric stretching vibrations
3199.81	O–H stretching vibrations
2723.96	CH_2 symmetric stretching vibrations
2643.93	CH_2 stretching vibrations
1635.82	NH_2 bending vibrations
1521.08	COO stretching vibrations
1445.39	NH_2 rocking vibrations
1395.73	C–O stretching vibrations
1342.7	CH_2 wagging vibrations
1139.72	NH_3 rocking vibrations
1043.78	CCN stretching vibrations
903.969	CC stretching vibrations
706.783	COO^- symmetric stretching vibrations
553.47	Wagging of CO_2 structure

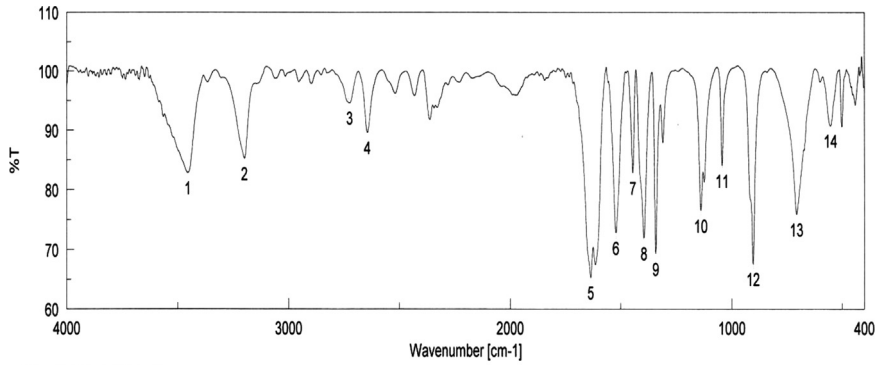

[Result of Peak Picking]

No.	Position	Intensity	No.	Position	Intensity	No.	Position	Intensity
1	3455.81	83	2	3199.81	85	3	2723.96	95
4	2643.93	90	5	1635.82	65	6	1521.08	73
7	1445.39	83	8	1395.73	72	9	1342.7	69
10	1139.72	76	11	1043.78	84	12	903.969	68
13	706.783	76	14	553.47	91			

Fig. 5. FTIR spectrum of DCDGZ II crystal.

3.3. Optical characterization

3.3.1. UV–vis–NIR absorption spectral studies

The UV–vis–NIR spectrum gives information about the structure of the molecule, because the absorption of UV and visible light involves the promotion of the electron in σ and π orbitals from the ground state to higher energy states. Transmission spectral analysis is important for any NLO materials as a non-linear optical material can be of practical use only if it has wide transparency window [26,27]. Optical absorption spectral analysis was done on the as grown DCDGZ II compound and the spectrum is shown in Fig. 6. It was noted that the lower UV cut-off of the crystal occurs at 240 nm. The transmission above 50% was observed from 300 nm to 2100 nm which clearly shows that the crystal possesses good optical transparency for the second harmonic generation of Nd^{3+}:YAG laser. This result is in good agreement with the reported value in reference [15].

3.3.2. Determination of optical band gap

The optical absorption coefficient (α) was calculated from the transmittance using the following relation,

$$\alpha = \frac{1}{d} \log \frac{1}{T} \tag{7}$$

where 'T' is the transmittance and 'd' is the thickness of the crystal.

Owing to the direct band gap, the crystal under study has an absorption coefficient (α) obeying the following relation for high photon energies ($h\nu$):

$$\alpha = \frac{A(h\nu - E_g)^{1/2}}{h\nu} \tag{8}$$

where E_g is the optical band gap of the crystal and A is a constant. The plot of variation of $(\alpha h\nu)^2$ vs $(h\nu)$ is shown in Fig. 7 and E_g is evaluated by the extrapolation of the linear part [28]. The band gap was found to be 2.2 eV. The colourless nature of the crystal shows its high transmission in the entire UV–Vis–NIR region and the obtained values are in good agreement with the reported values [29].

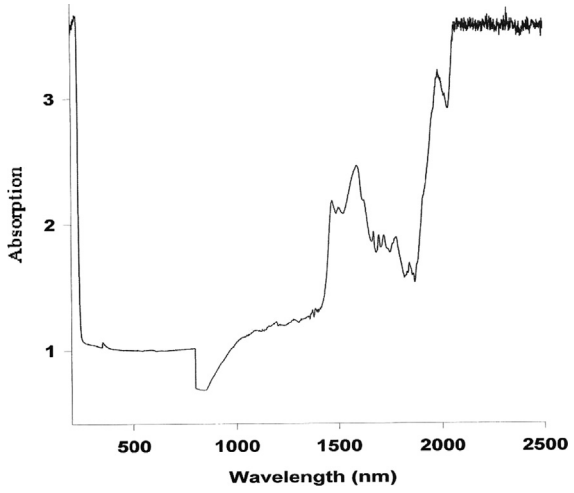

Fig. 6. Optical absorption spectrum of DCDGZ II crystal.

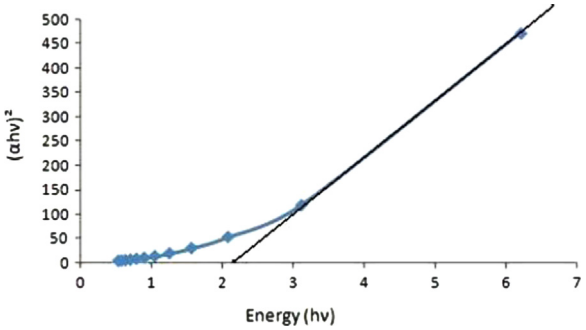

Fig. 7. Optical band gap of DCDGZ II crystal.

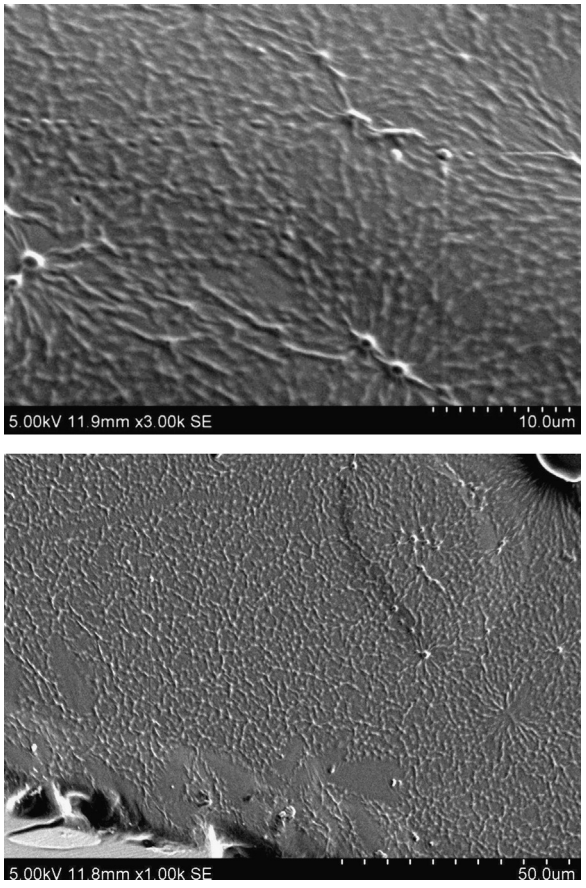

Fig. 8. SEM image of DCDGZ II crystal.

3.3.3. SEM analysis

Surface analysis of DCDGZ II was carried out using Hitachi-S-3400N scanning electron microscope and the SEM micrograph obtained was shown in Fig. 8. Gold carbon coating was given before subjecting the crystal surface to electron beam. The maximum magnification possible in the equipment is 3,00,000 times with a resolution of 10 nm. From the SEM image it is clear that the surface of the grown crystal appears smooth though it has pots and microcrystal on the surface. Overall the surface was very smooth with the appearance of few inclusions, formed on the crystal during growth and they

are influenced by the growth conditions. The grain boundaries are clearly seen which shows the perfect growth of the crystal.

3.4. TGA/DTA analysis

Thermogravimetric (TGA) and differential thermal analysis (DTA) provide information regarding phase transition, water of crystallization and different stages of decomposition of the crystal system [27]. The TGA of DCDGZ II crystal was carried out between 30 °C and 870 °C in the nitrogen atmosphere at a heating rate of 20 °C/min using TGA Q500 V20.10 Build equipment and the obtained spectrum is shown in Fig. 9. On a careful examination of this shows three stages of weight loss. The weight loss is found to be 10.95% at 200 °C, 32.18% at 400 °C and 37.88% at 860 °C.

The DTA analysis was also carried out in the same atmospheric condition. There is a sharp endothermic peak at 200 °C and it is assigned to the melting point of the title compound. It is followed by the decomposition and volatilization of the compound above 200 °C. Hence it may be useful for making the NLO devices below its melting point. This value of thermal stability was in contradictory with the values reported in Ref. [15], this may be due to the change in the water molecule present in the crystal structure. Thus the grown crystal shows a good thermal stability.

3.5. Dielectric measurements

3.5.1. Dielectric constant and dielectric loss measurements

The capacitance (C_{crys}) and dielectric loss ($\tan\delta$) were measured using the conventional parallel plate capacitor method with frequency range (50 Hz to 5 MHz) using Hioki-LCR Hi-Tester 3535 at various temperatures ranging from 313 K to 323 K. The dielectric studies of DCDGZ II crystals were performed by selecting high transparency rectangular shaped crystal plates of dimension $5.11 \times 2.01 \times 1.10\ mm^3$ and the sample was coated with good quality graphite to obtain a good conductive surface layer. In the observation it was found that there were sudden shoot-up's in dielectric constant (ξ_r) at lower frequencies (100 Hz). The dielectric constant has higher values in the lower frequency region and it decreases with the applied frequency (Fig. 10). The value of 'ξ' at lower frequency may be due to the presence of all the four polarizations namely space charge, orientational, electronic and ionic polarizations and its lower value at higher frequency was due to the loss of significance of these polarization gradually. The variation of dielectric constant as a function of temperature for varying frequencies is shown in Fig. 11. It shows that the crystal behaves as paraelectric before 318 K and becomes ferroelectric above 318 K, at varying frequencies. Thus the DCDGZ II crystal may exhibit ferroelectric nature at higher temperatures. The variation of dielectric loss with frequency is shown in Fig. 12. The ferroelectric nature of the crystal was proved by the P–E loop in Ref. [16], but the

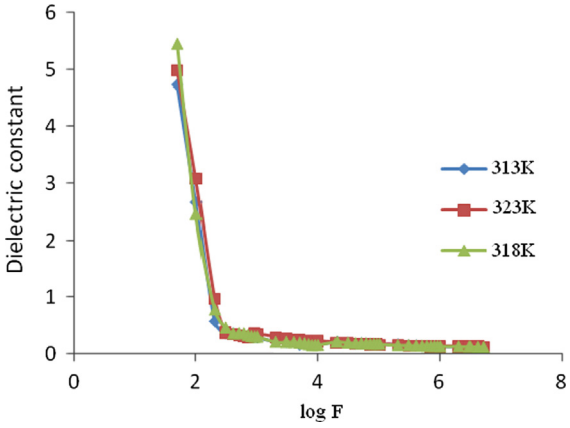

Fig. 10. Dielectric constant vs log F in DCDGZ II crystal.

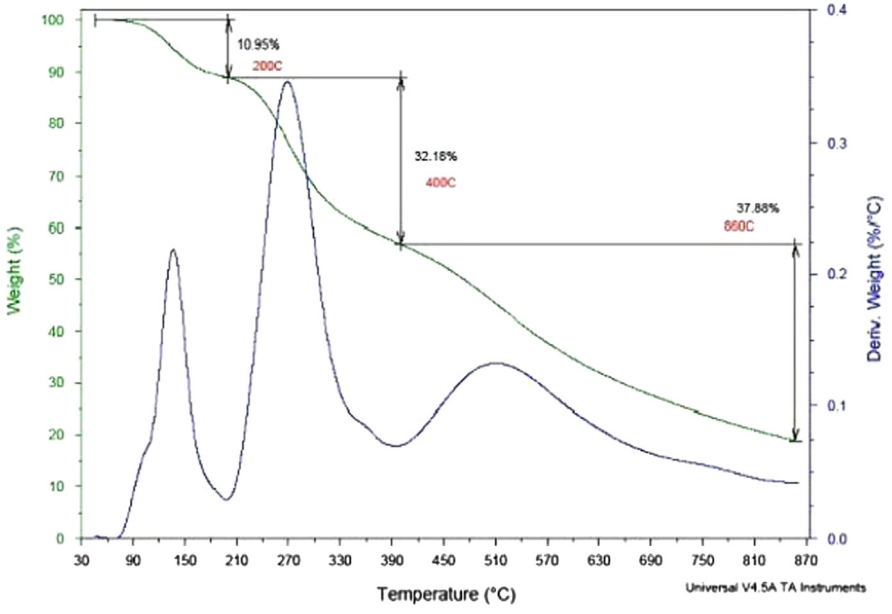

Fig. 9. Thermal analysis (TGA/DTA) of DCDGZ II crystal.

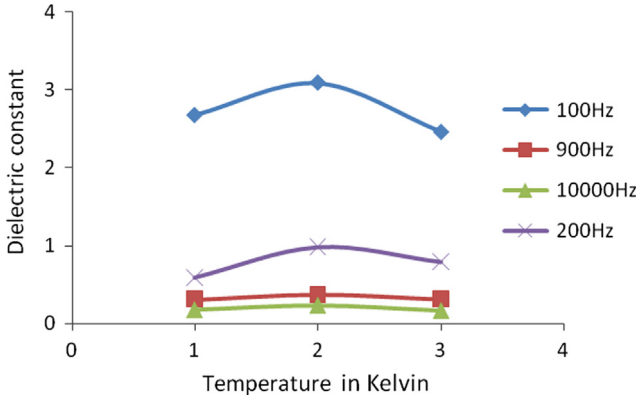

Fig. 11. Dielectric constant vs temperature in DCDGZ II crystal.

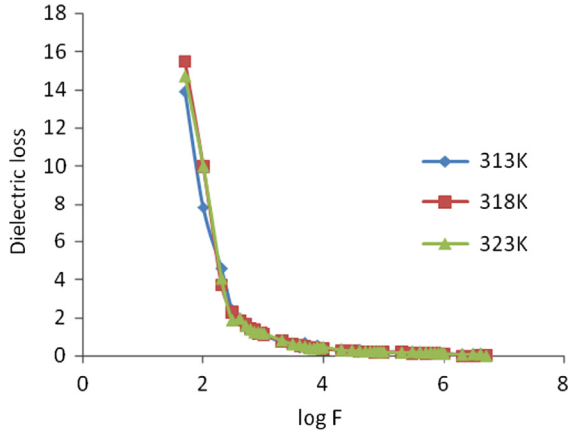

Fig. 12. Dielectric loss vs log F in DCDGZ II crystal.

transition temperature of it was found to be 363 K in the reference. The lower value of the dielectric loss with high frequency for this crystal suggests that the sample possesses enhanced optical quality with lesser defects and this parameter is a vital importance for non-linear optical material in their application [31].

3.5.2. *Electrical conductivity studies*

The dielectric constant was calculated using the relation

$$\varepsilon = \frac{Cd}{A\varepsilon_O} \tag{9}$$

where C is the capacitance, d is the thickness of the crystal, A is the area of the crystal and ε_O is the dielectric constant of free space.

The electrical conductivity in crystals gives an insight into the material properties with respect to transport of ions and electrons. It gives information regarding relaxation time, mobility and temperature dependence of these properties. The alternating current (ac) conductivity σ_{ac} is calculated using the relation [32]

$$\sigma_{ac} = 2\pi f \varepsilon_O \varepsilon' \tan\delta \tag{10}$$

where $\tan\delta$ is the dielectric loss measured directly from the impedance analyzer, f is the frequency of the applied ac field

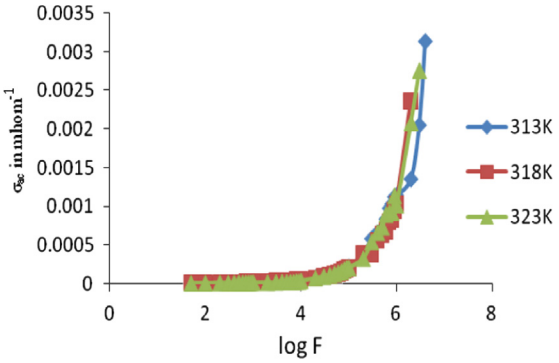

Fig. 13. Variation of ac conductivity with log F in DCDGZ II crystal.

(Hz). The variation of ac conductivity σ_{ac} with $\log F$ is depicted in Fig. 13.

It was observed that the crystal has very low conductivity in the low frequency region up to the frequency 50 Hz to 40 kHz for all temperatures. Thereafter the ac conductivity was found to be increasing feebly up to 4 MHz. Sharply at 4 MHz the conductivity increases abruptly for all the measured temperatures, which indicates the dielectric breakdown frequency of this material.

The dc electrical conductivity of the crystal at room temperature is evaluated using the relation

$$\sigma_{dc} = \frac{d}{AR_{dc}} \tag{11}$$

where R_{dc} is the total electrical resistance of the sample. The value of R_{dc} was evaluated from the Cole–Cole plots plotted between $Z' = Z\cos\theta$ (real part of impedance) and $Z'' = Z\sin\theta$ (imaginary part of impedance). The low value of electrical conductivity of DCDGZ II crystal was due to the decrease in mobility of the charge carriers by ion size, which brings changes in the electronic band structure. The Cole–Cole plots between the complex impedances of DCDGZ II crystal at various temperatures ranging from 313 K to 323 K are shown in Fig. 14. From these plots the bulk resistance (R_h) values were measured and it is quite evident that the bulk resistance decreases with increasing temperatures resulting in the enhancement of electrical conductivity at higher temperatures. The dc conductivity values calculated using Eq. (10) for various temperatures are presented in Table 6. dc conductivity vs temperature graph is shown in Fig. 15. The graph explains the increase in the conductivity with the increase in the temperature due to the increase in mobility and release of ions at elevated temperatures.

The activation energy of the crystal is also calculated from an Arrhenius plot using the relation

$$\sigma = \sigma_0 \exp\left(-\frac{E_a}{kT}\right) \tag{12}$$

where σ is the conductivity at temperature T, E_a the activation energy for the electrical process and k is the Boltzmann constant. The activation energy was obtained from the plot between $\log \sigma T$ ($\Omega^{-1}\,m^{-1}$) and $1000/T$ (K^{-1}) as shown in

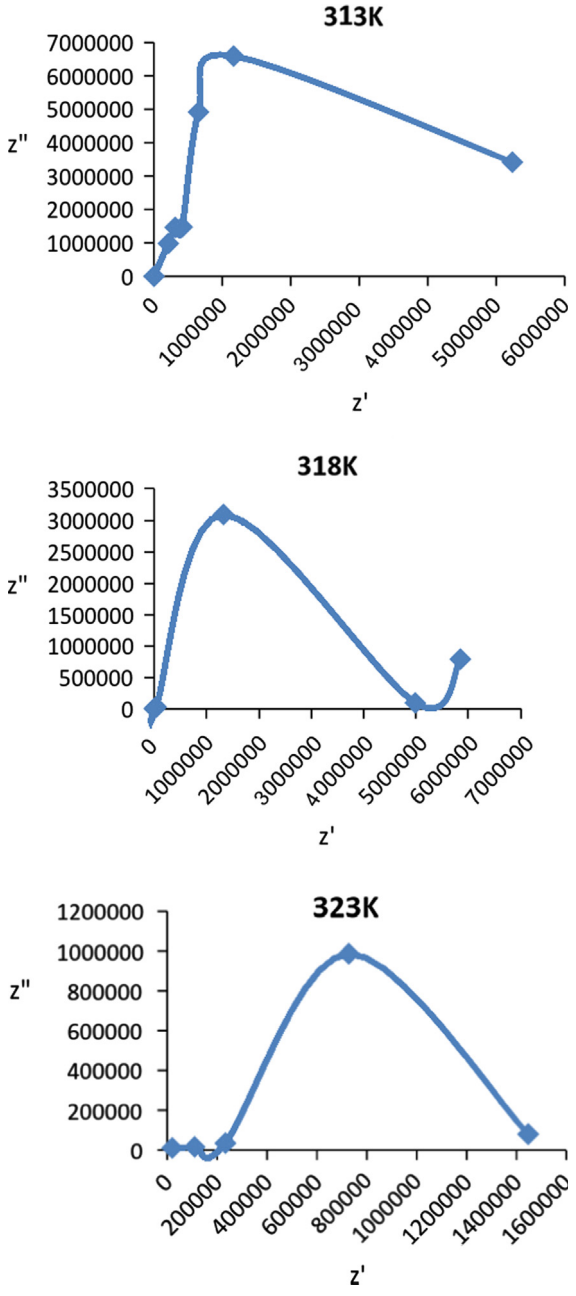

Fig. 14. Cole–Cole plots of DCDGZ II crystal.

Table 6
dc conductivity at various temperatures for DCDGZ II crystal

dc conductivity (mho m^{-1})	Temperatures (K)
2.05×10^{-5}	313
2.15×10^{-5}	318
7.4×10^{-5}	323

Fig. 16. The activation energy calculated from the slope of the curve was found to be $E_a = 0.547$ eV. A similar range of activation energy values have been reported for some super-ionic conductors [33], which infer that DCDGZ II crystal will behave at high temperatures as a super-ionic conductor.

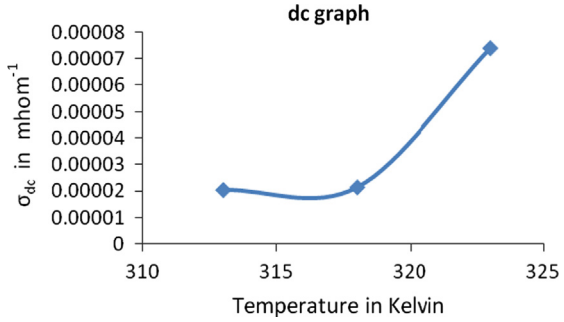

Fig. 15. Variation of dc conductivity with temperature.

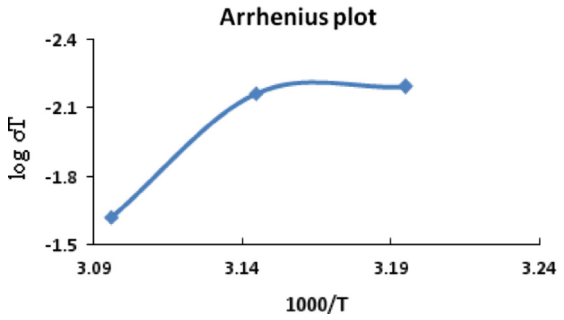

Fig. 16. log σT vs 1000/T in DCDGZ II crystal.

Table 7
Comparison of SHG efficiency of DCDGZ II crystal with other similar centrosymmetric crystals.

Crystal	Space group	SHG efficiency	Reference
(p-Nitrophenol hexa methylene tetramine phosphoric acid water) super molecular crystal	$P2_1/c$	4.1	[30]
R,D-serine	$P2_1/a$	0.2	[31]
Glycine picrate	$P2_1/a$	2.34	[32]
Monohydrate piperazine hydrogen phosphate	$P2_1/c$	0.68	[33]
Picolium maleate	$P2_1/c$	0.4	[34]
DCDGZ II	$C2_1/c$	0.888	Present

3.6. NLO studies

The NLO property of DCDGZ II crystal was determined using Kurtz and Perry [34] second harmonic generation (SHG) test. The grown crystal of DCDGZ II was powdered with a uniform particle size and packed in a micro-capillary of uniform bore. The crystal then exposed to Q-switched Nd–YAG laser radiations of wavelength 1064 nm with pulse width of 8 ns and repetition rate of 10 Hz. The generation of second harmonic was confirmed by the emission of green light. For SHG studies the input beam energy used was 8.8 mJ/pulse and the SHG signal outputs are 45 mV and 40 mV for KDP and DCDGZ II respectively. The SHG conversion efficiency of DCDGZ II crystal was found to be about 0.888 times that of KDP. Some of the earlier reported centrosymmetric crystals with the similar type of space group and SHG efficiency are given as comparison in Table 7 [35–39]

4. Conclusion

Dichloro-diglycine zinc II (DCDGZ II) single crystals were grown by slow solvent evaporation technique. The crystallinity of the grown crystal was confirmed by single crystal X-ray diffraction analysis and the structure of the crystal was solved. The theoretical calculations were carried out and the calculated values of the polarizability were compared with the values of polarizability using Clausius–Mossotti equation which agrees well with it. Various functional groups present in the grown crystal were identified by FTIR spectrum. The optical quality of the grown crystal was justified using SEM and optical absorption studies. The lower cut off wavelength was found to be 240 nm. Thermal stability of the grown crystal was studied by TG and DTA analyses shows that the crystal has a high thermal stability and is due to the presence of single water molecule in the grown crystal. The dielectric studies were also carried out. The crystal possesses ferroelectric transition at 318 K which was already proved by the P–E loop at 363 K. The low value of the dielectric loss with high frequency for this crystal suggests that the sample possess enhanced optical quality with lesser defects and this parameter is a vital importance for non-linear optical material in device applications. The variation of the electrical conductivity with the temperatures was studied using Cole–Cole plots. The Arrhenius plot confirms that the activation energy was found to be $E_a = 0.547$ eV and infer that DCDGZ II crystal will act in between super-ionic conductor and dielectric. The property of the SHG measurements of the crystal confirms the non-linear nature and the SHG efficiency is found to be 0.888 times that of KDP.

Acknowledgement

One of the authors (B. Uma) is grateful to Prof. P.K. Das, Department of Inorganic and Physical chemistry, Indian Institute of Science, Bangalore for having extended the laser facilities for the SHG measurement. The author also acknowledges the Department of Chemistry, I.I.T., Madras for providing the UV, TGA/DTA and FTIR facilities. The author extends her thanks to the Department of Mechanical engineering, Anna University for providing the SEM facility. One of the authors (Rajnikant) acknowledges the Department of Science & Technology, University of Jammu for single crystal X-ray diffractometer as a National Facility under Project no. SR/S2/CMP-47/2003.

References

[1] Yun Zhang, Hua Li, Bin Xi, Yunxia Che, Jimin Zheng, J. Mater.Chem. Phys. 108 (2008) 192–195.
[2] S. Natarajan, S.A. Martin Britto, E. Ramachandran, J. Cryst. Growth Des. 6 (1) (2006) 137–140.
[3] Zhihua Sun, Guanghui Zhang, Xinqiang Wang, Zeliang Gao, Xiufeng Cheng, Shaojun Zhang, X.u. Dong, J. Cryst. Growth Des. 9 (7) (2009) 3251–3259.
[4] K. Kirubakaran, K. Selvaraju, R. Valluvan, N. Vijayan, S. Kumararaman, J. Spect. Chem. Act., A 69 (2008) 1283–1286.
[5] B. Milton Boaz, S. Jerome Das, J. Cryst. Growth 279 (2005) 383–389.
[6] K. Parasuraman, K. Sakthi murugesan, R. Uthrakumar, S. Jerome Das, B. Milton Boaz, Physica B 406 (20) (2011) 3856–3860.
[7] B. Milton Boaz, J. Mary Linet, Babu Varghese, M. Palanichamy, S. Jerome Das, J. Cryst. Growth 280 (2005) 448–451.
[8] B. Milton Boaz, M. Palanichamy, Babu Varghese, C. Justin Raj, S. Jerome Das, Mater. Res. Bull. 43 (12) (2008) 3587–3595.
[9] R. Rajasekaran, P.M. Ushasree, R. Jayavel, P. Ramasamy, J. Cryst. Growth 229 (2001) 563–567.
[10] K. Ambujam, K. Rajarajan, S. Selvakumar, J. Madhavan, Gulam Mohamed, P. Sagayaraj, Opt. Mater. 29 (2007) 657–662.
[11] S. Natarajan, C. Muthukrishnan, S.A. Bahadur, R.K. Rajaram, S.S. Rajan, J. Z. Kristallogr. 198 (1992) 265–270.
[12] M.J. Buerger, R. Barney, T. Hahn, J. Z. Kristallogr. 108 (1956) 130–144.
[13] P. Piret, J. Meunier-Piret, J. Verbist, M. Van Meerssche, J. Bull. Soc. Chim. 81 (1) (1972) 539–546.
[14] S.C. Bhattacharyya, N.N. Saha, J. Cryst. Mol. Struct. 8 (1978) 209–215.
[15] J. Mary Linet, S. Jerome Das, Phys. B 406 (2011) 836–840.
[16] S. Suresh, A. Ramanand, D. Jayaraman, S.M. Priya, R. Vasanthakumari, J. Miner. Mater. Charact. Eng. 10 (4) (2011) 339–349.
[17] S. Mary Navis Priya, B. Varghese, J. Mary Linet, G. Bhagvannarayana, C. Justin Raj, S. Krishnan, S. Dinakaran, S. Jerome Das, J. Cryst. Growth Des. 8 (5) (2008) 1663–1667.
[18] M. Senthil Pandian, P. Ramasamy, J. Cryst. Growth 312 (2010) 413–419.
[19] A.A. Chernov, Oxford Diffraction, Oxford Diffraction Ltd, Yarnton, Oxfordshire, England, 2010.
[20] G.M. Sheldrick, Acta Crystallogr. A64 (2008) 112–122.
[21] L.J. Farrugia, J. Appl. Cryst. 30 (1997) 565.
[22] M. Nardelli, J. Appl. Cryst. 28 (1995) 659.
[23] A.L. Spek, X- ray crystal study and molecular symmetry, University of Utrecht, The Netherlands, 1999.
[24] N.M. Ravindra, R.P. Bharadwaj, K. Sunil Kumar, V.K. Srivastava, J. Infrared Phys. 21 (1981) 369.
[25] N.M. Ravindra, V.K. Srivastava, J. Infrared Phys. 20 (1980) 67–69.
[26] K. Machida, A. Kagayama, Y. Salto, Y. Kuroda, T. Uno, J. Spectrochim. Acta 33A (1977) 569.
[27] R. Sankar, R. Muralidharan, C.M. Raghavan, R. Jayavel, Mater. Chem. Phys. 107 (2008) 51–56.
[28] A.K. Chawla, D. Kaur, R. Chandra, Opt. Mater. 29 (2007) 995–998.
[29] B. Narayana Moolya, S.M. Darmaprakash, J. Cryst. Growth 293 (2006) 86–92.
[30] F.Q. Meng, M.K. Lu, Z.H. Yang, H. Zeng, Mater. Lett. 33 (1998) 265–268.
[31] Charoen-In Urit, P. Ramasamy, P. Manyum, J. Cryst. Growth 312 (2010) 2369–2375.
[32] Banwari Lal, K.K. Barnzai, P.N. Kotru, B.M. Wanklyn, Mater. Chem. Phys. 85 (2004) 353–365.
[33] J.N. Babu Reddy, S. Vanishri, Ganesh Kamath, Suja Elizabeth, H.L. Bhat, D. Isakov, M. Belsley, E. de Matos Gomes, T.L. Aroso, J. Cryst. Growth 311 (2009) 4044–4049.
[34] S.K. Kurtz, T.T. Perry, J. Appl. Phys. 39 (1968) 3798–3813.
[35] T. Ishihara, K. Koshino, H. Nakashima, J. Phys. Rev. Lett. 91 (2003) 1–4.
[36] Anna Somac, Marek Samoc, Verselin Z. Kotev, Barry Luther-Davies, Proceedings of the Symposium on Photonics Technologies for 7th Framework Program, Wroclaw, 2006, pp. 250–253.
[37] Mohd Shakir, S.K. Kushwaha, K.K. Maurya, Manju Arora, G. Bhagavannarayana, J. Cryst. Growth 311 (2009) 3871–3875.
[38] P. Krishnana, K. Gayathri, G. Bhagavannarayana, S. Gunasekaran, G. Anbalagan, J. Spectchim. Acta Part A 102 (2013) 379–385.
[39] P. Pandi, G. Peramiyan, S. Sudhakar, G. Chakkaravarthi, R. Mohankumar, G. Bhagavannarayana, R. Jayavel, J. Spectchim. Acta Part A 98 (2012) 7–13.